

# A Comparative Study of Adversarial Attacks against Point Cloud Semantic Segmentation

Jiacen Xu<sup>1</sup>, Zhe Zhou<sup>2</sup>, Boyuan Feng<sup>3</sup>, Yufei Ding<sup>3</sup>, and Zhou Li<sup>1</sup>

<sup>1</sup>University of California, Irvine

<sup>2</sup>Fudan University

<sup>3</sup>University of California, Santa Barbara

**Abstract**—Recent research efforts on 3D point cloud semantic segmentation (PCSS) have achieved outstanding performance by adopting deep CNN (convolutional neural networks) and GCN (graph convolutional networks). However, the robustness of these complex models has not been systematically analyzed. Given that PCSS has been applied in many safety-critical applications (e.g., autonomous driving, geological sensing), it is important to fill this knowledge gap, in particular, how these models are affected under adversarial samples. While adversarial attacks against point clouds have been studied, we found many questions remain about the robustness of PCSS. For instance, all the prior attacks perturb the point coordinates of a point cloud, but the features associated with a point are also leveraged by some PCSS models, and whether they are good targets to attack is unknown yet.

We present a comparative study of PCSS robustness in this work. In particular, we formally define the attacker’s objective under targeted attack and non-targeted attack and develop new attacks considering a variety of options, including feature-based and coordinate-based, norm-bounded and norm-unbounded, etc. We conduct evaluations with different combinations of attack options on two datasets (S3DIS and Semantic3D) and three PCSS models (PointNet++, DeepGCNs, and RandLA-Net). We found all of the PCSS models are vulnerable under both targeted and non-targeted attacks, and attacks against point features like color are more effective. With this study, we call the attention of the research community to develop new approaches to harden PCSS models against adversarial attacks.

**Index Terms**—Point Cloud, Semantic Segmentation, Adversarial Attack

## I. INTRODUCTION

3D point cloud semantic segmentation (PCSS) aims to assign a class label to each embedded 3D point in a scene, which has been playing an increasingly important role in many real-world applications, like autonomous driving and geological sensing. Due to the data complexity, deep-learning models based on CNN and GCN have been extensively leveraged for this task [15], [16], [39].

Due to their usage of point cloud in safety-critical applications, a number of works have attempted to generate adversarial examples against point cloud models, which migrate the existing attacks against 2D images, like FGSM, iFGSM, PGD and CW, to the 3D point cloud setting [13], [20], [21], [36], [40], [42], [43], [45], [48], [49]. However, we found all of them focused on the task of *objection recognition*, in which one class label is assigned to the *whole* point cloud.

Though objection recognition is an important task performed by the point cloud models, semantic segmentation

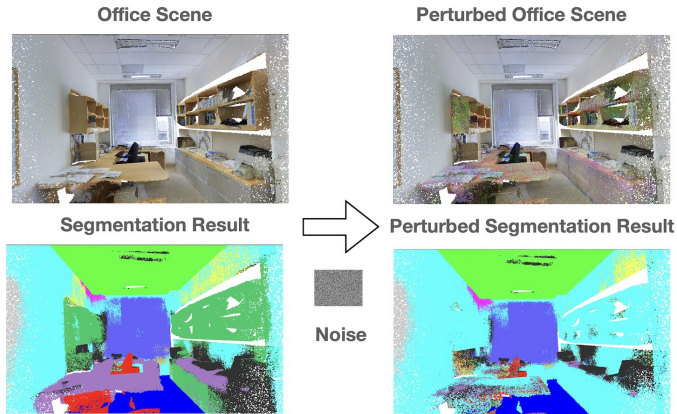


Fig. 1. One example of S3IDS dataset after color-based perturbation under the targeted attack setting. Different objects are colored differently. Multiple objects (desk, chair, and bookcase) are misclassified after the attack.

is probably performed more broadly, as it processes a *real-world scene* which often contains many objects. As far as we know, the work from Zhu et al. [52] is the only one attacking PCSS models, but it is only tested under the setting of LiDAR sensing, and only one outdoor dataset is evaluated. Hence, the robustness of PCSS models under the adversarial samples have not been systematically explored, and there is an urgent need to answer questions like which PCSS model design is more robust and in what setting (e.g., indoor or outdoor) the attack is more likely to succeed.

Yet, answering these questions is non-trivial, if directly applying the adversarial perturbation against 2D images or point cloud object recognition to PCSS. First, in the segmentation task, the class label is assigned to *every* point, and the segmentation result of a point is also determined by its surrounding points, which increases the uncertainty of the attack outcome. Second, various data pre-processing procedures such as random filtering, nodes copying, and point clouds separation have been applied by the PCSS models, and the attack accuracy can be impacted by them. Finally, perturbation is only performed on the point coordinates by prior works, but there are other point features are used for semantic segmentation. For instance, 9 features are included in a point cloud of the S3IDS dataset [44] and 6 features are

included in Semantic3D dataset [11]. Whether and how the features undermine the robustness of the PCSS models have not been studied.

**Our Study.** We perform the first systematic and comparative analysis on the robustness of PCSS, by developing a *holistic* attack framework that incorporate different attack configurations. We first convert attacker’s objectives under targeted and non-targeted settings into the forms that can be solved through optimization. Under each objective, we develop a norm-bounded attack method adjusted from NB and a norm-unbounded one adjusted from NU, to compare their effectiveness. In addition to attacking point coordinates like previous point cloud attacks, we customize the attack methods to exploit the point features like color channels. Hence, our attack framework supports 8 attack configurations (targeted/non-targeted  $\times$  norm-bounded/norm-unbounded  $\times$  coordinate-based/color-based), which enables a comprehensive analysis of PCSS models.

**Evaluation Results.** We evaluate the attack framework against three popular PCSS models, including ResGCN-28 [16], PointNet++ [29] and RandLA-Net [12], as they represent different directions in processing point cloud. For the datasets, we use S3IDS and Semantic3D, representing both indoor and outdoor scenes. Below we highlight key findings:

(1) We compare the perturbation on point features (color in particular) against point coordinates, and our result shows that color features are more vulnerable.

(2) Under the non-targeted attack, we found all tested PCSS models are vulnerable, with the norm-unbounded attack being more effective (e.g., dropping the segmentation accuracy from *from 85.90% to 6.75%* when attacking ResGCN-28). In the meantime, the perturbation added to the original point cloud is still small, measured by  $L_2$  distance. Notably, PointNet++, ResGCN-28, and RandLA-Net belong to very different model families, suggesting our developed attacks are universally effective.

(3) For the targeted attack, as the attacker needs to select the source objects and determine what they should be changed to, the selection makes a big difference, as some objects are easier to manipulate (e.g., changing board to wall in S3IDS). Figure 1 shows an example of the targeted attack.

(4) The outdoor scenes are similarly vulnerable comparing to the indoor scenes (e.g., accuracy drops from 98.25% to 16% when RandLA-Net is used to segment Semantic3D point cloud).

(5) The adversarial examples generated against one model have good transferability.

Overall, our study demonstrates that the robustness of the deep-learning models under PCSS is questionable, and we outline a few directions for improving their robustness.

**Contributions.** Below we summarize the main contributions of this work.

- We develop a holistic framework to enable various attack configurations against PCSS.

- We extend the previous attacks that are coordinate-based to feature-based.
- We evaluate different attack configurations against different PCSS models and datasets.
- Our code will be made publicly available in a GitHub repository.

**Roadmap.** Section II discusses the background and the related works from deep learning on point clouds and adversarial examples. We formulate the problem of adversarial attacks against PCSS in Section III. The design of attack methods is elaborated in Section IV. We show the results in Section V. In Section VI, we discuss the potential defenses and limitations of this work, and Section VII concludes the paper.

## II. BACKGROUND AND RELATED WORKS

### A. Deep Learning on Point Cloud

3D point cloud generated by sensors has become a popular medium to represent the surrounding environment, which has been extensively used in the domain of computer vision and autonomous driving. Two primary tasks have been explored with point clouds, namely objection recognition (or classification), and semantic segmentation. We focus on the second task.

To process the data stored in a point cloud, early works transformed the data into regular 3D voxel grids or images for the conventional CNN, which makes the data unnecessarily voluminous. PointNet [28] addressed this issue by using a shared Multilayer perceptron (MLP) on every individual point, and a global max-pooling to convert the input into a fixed-length feature vector. Since then, variations like PointNet++ [29], Sonet [17], PointCNN [19], KPConv [35], PointNeXt [30] have been proposed to use sophisticated modules and hierarchical architectures to aggregate local neighborhood information and extract local structure.

Besides CNN, DeepGCN [16] shows that GCN can be leveraged to process point clouds. It solves the gradient vanishing problem when models become deeper, as the data is sparse in the geometry space but nodes in adjacency have strong relations.

A major drawback of many point cloud models is that the pre-processing and voxelization steps are too computation-intensive for large point clouds. To address this issue, RandLA-Net [12] leveraged random point sampling and local feature aggregation, and showed 200 $\times$  speedup. The large outdoor dataset like Semantic3D can be handled efficiently.

In this work, we evaluate the point cloud models from the aforementioned three directions, including PointNet++ under CNN, ResGCN under GCN, and RandLA-Net under point sampling.

Recently, some techniques are proposed to improve the performance of semantic segmentation in particular, including contrastive boundary learning for better scene boundary analysis [34] and multi-view aggregation to leverage the information from the associated 2D images [31]. Other deep models like GAN [32] and transformer [23], [46] have been to process

point cloud. We found their adoption is still at the early stage and leave the evaluation on them as future works.

### B. Adversarial Examples

The output of a point cloud model can be manipulated under adversarial examples. In the setting of 3D point cloud, existing works [13], [20], [21], [36], [40], [42], [43], [45], [48], [49] took a gradient-based approach to generate adversarial examples by perturbing the coordinates of a point or adding/removing a point. GAN has also been used to create adversarial examples [50]. The popular methods in attacking CNN that handles 2D images, including FGSM [10], iFGSM [14], PGD [22], and CW [6], have been applied. However, these works aim to fool object recognition, which is a different task from this paper’s focus.

Though attacks against semantic segmentation have been explored, most of the existing works [3], [25], [26] generate adversarial examples against *2D images*, which have very different properties compared to 3D point clouds. The closest work comes from Zhu et al. [52], which attacked LiDAR PCSS. Yet, since it focused on autonomous driving, only one outdoor dataset is evaluated and the perturbation is only applied to the coordinates. We believe the robustness of PCSS models has not been systematically evaluated, as PCSS can be used by applications other than autonomous driving (e.g., indoor navigation) and point features could also play an important role in addition to coordinates. In fact, we found models like RandLA-Net and PointNet++ extensively leverage point features to boost the accuracy. In this paper, we make the *first* attempt to comparatively analyze the robustness of PCSS, in order to fill this knowledge gap.

### C. Point Cloud Datasets

To evaluate the performance of point cloud models, a number of public datasets have been released. For object classification, ModelNet [41], ScanObjectNN [38], ShapeNet [7] and PartNet [24] are widely used. For semantic segmentation, S3DIS [2], Semantic3D [11] and KITTI [4] are the major datasets. Different datasets are created for object classification and semantic segmentation because the number of objects and labels differ: a scene for objection recognition has only one object and one label, while a scene for semantic segmentation usually has multiple objects and labels. It is also more challenging to perform semantic segmentation, as the classification result on one object can be impacted by the nearby objects in the same scene and some objects might only have a partial outline in the scene.

In the paper, we select S3DIS and Semantic3D as the datasets to evaluate our attacks in both indoor and outdoor scenes. They both contain coordinate and color, which enables a fair assessment of the attack effectiveness on these two fields.

## III. PROBLEM FORMULATION

**Symbols.** In this section, we give a formal definition of point clouds and the attacker’s goals. Table I lists the main symbols used in this paper and their description.

TABLE I  
MAIN SYMBOLS USED IN THE PAPER.

Symbol	Description
$X$	a point cloud
$Y$	the labels of all points in the point cloud
$x_i$	a point
$y_i$	a class label on $x_i$
$p_i$	the coordinates of $x_i$
$c_i$	the features of $x_i$
$R$	the perturbation values on the point cloud
$r_i$	the perturbation values on $x_i$
$T$	the set of point indices
$\mathcal{F}_\theta(\cdot)$	the model for PCSS
$Z(\cdot)_i$	the logits of the model’s prediction
$\mathcal{T}(\cdot)$	the function selecting a subset of $X$ or $Y$
$\mathcal{D}(\cdot)$	the distance function
$\mathcal{S}(\cdot)$	the smoothness penalty
$\mathcal{L}(\cdot)$	the loss function
NB	Norm-bounded attack
NU	Norm-unbounded attack

A point cloud can be defined as a set of  $N$  points, i.e.,  $\{p_i\}_{i=1}^N$ , where each point  $p_i = (pos_x, pos_y, pos_z)$ , representing the 3D coordinates of a point. This basic form is usually sufficient for single-object recognition [28], [29]. For semantic segmentation, auxiliary features of a point like color can be leveraged, which can be obtained from a multi-spectral LiDAR for example. We denote the features associated with a point  $p_i$  as  $c_i$ , so a point cloud  $X = \{x_i | i = 1 \dots N, x_i = \{p_i, c_i\}\}$  where  $c_i = (feat_1, feat_2, \dots, feat_k)$  for  $k$  features.

We assume the adversary has white-box access to the model to be attacked. In other words, the adversary has full access to the model’s structure and parameters. The perturbation happens on the model input in the test time which is also known as the evasion attack. We study two types of attack: *targeted* attack and *non-targeted* attack. Below we formalize their goals.

First, we assume  $\mathcal{F}_\theta : \mathcal{X} \rightarrow \mathcal{Y}$  is the segmentation model which maps an input point cloud  $X = \{x_i | i = 1 \dots N, x_i \in \mathcal{X}\}$  to the labels of *all points*  $Y = \{y_i | i = 1 \dots N, y_i \in \mathcal{Y}\}$ .  $\mathcal{X}$  is the universe of points, and  $\mathcal{Y}$  is the universe of class labels, e.g., desk, wall, and chair. We design methods under both norm-bounded and norm-unbounded principles for the targeted and the non-targeted attack.

**Targeted Attack.** In this setting, the adversary chooses a subset of points  $X_T = \{x_i | i \in T, x_i \in X\}$ , where  $T$  is the set of indices, and perturbs  $X_T$  to change their predicted labels to  $Y_T = \{y_i | i \in T, y_i \in \mathcal{Y}\}$ . For a point  $x_i = \{p_i, c_i\}$ , we assume the attacker either perturbs its coordinates  $p_i$  or its features  $c_i$ . We treat coordinates and features separately as the perturbation methods have to be designed differently under their unique constraints. The perturbation values on the original point cloud  $X$  can be represented as  $R = \{r_i | i \in T\}$ , and the new point cloud will be  $X' = \{x_i | i \notin T, x_i \in X\} + \{x_i + r_i | i \in T, x_i \in X\}$ . Under coordinate-based perturbation,  $r_i = \{r_{p_i}, 0^k\}$ , where  $r_{p_i}$  denotes the changes on the 3D coordinates. Under feature-based perturbation,  $r_i = \{0^3, r_{c_i}\}$ , where  $r_{c_i}$  denotes the changes on the  $k$  features.

We first consider the norm-bounded attack, by which the

attacker tries to minimize the difference between the predicted labels on  $X_T$  and the targeted labels  $Y_T$ , while the perturbation is bounded by  $\epsilon$ . Hence, the attacker’s goal can be formalized as:

$$\arg \min_R \mathcal{L}_T(X', Y_T), \text{ s.t. } \mathcal{D}(R) \leq \epsilon \quad (1)$$

Here,  $\mathcal{D}(\cdot)$  is the distance function measuring the magnitude of the perturbation  $R$ .  $\mathcal{L}_T(\cdot)$  is the adversarial loss that measures the effectiveness of the attack. Notably, the attacker’s goal is quite different from the attacks against single-object recognition [42], where one label is assigned to the whole point cloud (i.e., the cardinality of  $Y'$  is 1) and the number of points after perturbation can differ (i.e.,  $X'$  and  $X$  have different cardinalities).

Under the norm-unbounded attack, the attacker tries to find the minimum perturbation values that can change the labels of  $X_T$  to  $Y_T$ . Hence, the attacker’s goal can be formalized as:

$$\arg \min_R \mathcal{D}(R), \text{ s.t. } \mathcal{T}(\mathcal{F}_\theta(X'), T) = Y_T \quad (2)$$

Where  $\mathcal{T}(\cdot)$  selects the prediction results indexed by  $T$  from  $X'$ .

Directly solving Equation 2 is difficult because the constraint  $\mathcal{T}(\mathcal{F}_\theta(X'), T) = Y_T$  is non-differentiable [6]. As a result, we reformulate Equation 2 to enable gradient-based optimization by introducing  $\mathcal{L}_T(\cdot)$  to replace this constraint, as shown in Equation 3. Besides, we add a smoothness penalty  $\mathcal{S}(\cdot)$  to encourage the optimizer to keep  $X'$  smooth, i.e., that the differences between the neighboring points are not drastic.

$$\arg \min_R \mathcal{D}(R) + \lambda_1 \cdot \mathcal{L}_T(X', Y_T) + \lambda_2 \cdot \mathcal{S}(X') \quad (3)$$

Where  $\lambda_1$  and  $\lambda_2$  are pre-defined hyper-parameters.

**Non-targeted Attack.** In this setting, the adversary does not have a specific target  $Y_T$ , but just manipulates the prediction  $\mathcal{F}_\theta(X')$  to be different from the ground-truth labels of all points in  $X_T$  (termed  $Y_{GT}$ ). Under norm-bounded attack, the attacker’s goal can be adjusted from Equation 1 to:

$$\arg \max_R \mathcal{L}_{NT}(X', Y_{GT}), \text{ s.t. } \mathcal{D}(R) \leq \epsilon \quad (4)$$

Where  $\mathcal{L}_{NT}(\cdot)$  is the adversarial loss regarding  $Y_{GT}$ .

Under norm-unbounded attack, the attacker’s goal can be adjusted from Equation 3 to:

$$\arg \max_R \mathcal{D}(R) + \lambda_1 \cdot \mathcal{L}_{NT}(X', Y_{GT}) + \lambda_2 \cdot \mathcal{S}(X') \quad (5)$$

#### IV. ATTACK DESIGN

In this section, we describe the design of the attacks under different goals described in Section III. Below we first describe the components used by the attacks. Then, we describe the attack workflows, which mainly differ by norm-bounded and norm-unbounded attacks.

As reviewed in Section II, none of the prior attacks against PCSS consider the point features, so we highlight the design of feature-based attacks here. In particular, we select the *color* features as the perturbation target, which turns  $c_i$  to

( $color_r, color_g, color_b$ ) for the three color channels, where  $color_*$  is the pixel value. We focus on the color channels as previous color-based attacks against 2D images show they are physically realizable, e.g., with carefully-printed stickers on the surface [9], and robust against surrounding illuminations, viewing angle, and distance [9], [47]. On the other hand, perturbing the point coordinates at pixel granularity in the physical world could be more challenging [5], [37].

##### A. Attack Components

Here we elaborate the distance function  $\mathcal{D}(\cdot)$ , adversarial loss functions  $\mathcal{L}_T(\cdot)$  and  $\mathcal{L}_{NT}(\cdot)$ , smoothness penalty  $\mathcal{S}(\cdot)$ , which are all listed in Section III.

**Distance Function.** When the color-based attack is chosen, we use  $L_2$  distance to measure the magnitude of the perturbation, as shown by Equation 6, because  $L_2$  distance is commonly used by 2D image models [6].

$$\mathcal{D}(R) = \sum_{i \in T} \|r_{c_i}\|_2^2 \quad (6)$$

As pointed out by [6], optimization on  $c_i$  encounters a box constraint, which is hard to solve. Hence, we map  $c_i \in [a, b]$  to a new variable  $W_i$ , and perform optimization over  $w_i$ , as shown in Equation 7.

$$r_{c_i} = a + \frac{b-a}{2} (\tanh(w_i) + 1) \quad (7)$$

Here  $\tanh(\cdot)$  makes the gradient smoother and always falls in  $[-1, 1]$ , so the optimizer could find the right perturbation sooner.  $a$  and  $b$  are adjusted based on the normalized value range of the PCSS model.

When the coordinate-based attack is chosen, we use  $L_0$  distance, i.e., how many points are changed, and the distance can be represented as:

$$\mathcal{D}(R) = \sum_{i \in T} \|r_{p_i}\|_0 \quad (8)$$

We use  $L_0$  distance since other distance metrics like  $L_2$  and  $L_\infty$  yield different value ranges based on the input range of coordinates. Specifically, a color channel has a fixed range from 0 to 255 regardless of the point clouds, but a coordinate can have different value ranges for different point clouds. Equation 7 is also applied on the coordinate for the ease of optimization.

**Smoothness Penalty.** The penalty is designed to make  $X'$  smooth. In Equation 9, the distance between each point and its top  $\alpha$  nearest neighbors is encouraged to be minimized.

$$\mathcal{S}(X', \alpha) = \sum_{x'_i \in X'} \sum_{x'_j \in \text{NB}(x'_i, \alpha)} (\|x'_i - x'_j\|_2) \quad (9)$$

Where  $\text{NB}(x'_i, \alpha)$  returns the top  $\alpha$  nearest neighbors. Noticeably, we consider all points rather than only points in  $X_T$ .

**Adversarial Loss.** We use the logits (the output of the layer before the last softmax layer) of  $\mathcal{F}_\theta$  to represent the adversarial

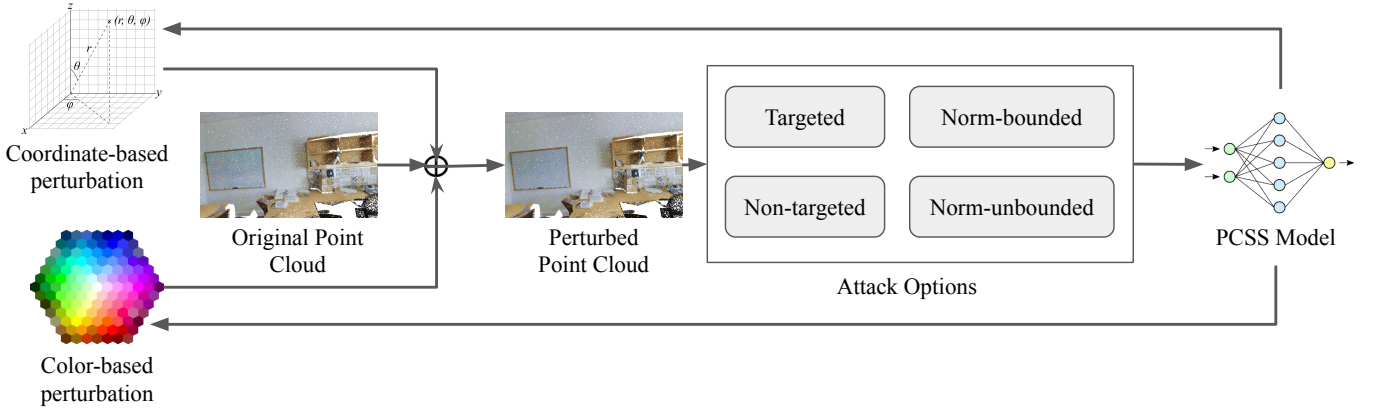


Fig. 2. The overall attack workflow.  $Y_T$  and  $Y_{GT}$  mean the target labels for the targeted attack and ground truth labels for the non-targeted attack.

loss for the targeted attack. This loss encourages the optimizer to minimize the logits of the class rather than the target label.

$$\mathcal{L}_T(X', Y_T) = \sum_{\substack{x'_i \in X' \\ y_i \in Y_T}} \max(\max_{j \neq y_i} (Z(x'_i)_j) - Z(x'_i)_{y_i}, 0) \quad (10)$$

Where  $Z(\cdot)_j$  represents the  $j^{\text{th}}$  element of the logits of the adversarial example, and  $Z(x'_i)_{y_i}$  means the target label's logits for  $x'_i$ . The largest logit that is not related to the target label is derived by  $\max_{j \neq y_i} (Z(x'_i)_j)$ .

For non-targeted attacks, the adversarial loss is adapted to encourage the prediction of points to be any class other than the ground-truth classes. The loss function can be changed from Equation 10 to:

$$\mathcal{L}_{NT}(X', Y_{GT}) = \sum_{\substack{x'_i \in X' \\ y_i \in Y_{gt}}} \max(Z(x'_i)_{y_i} - \max_{j \neq y_i} (Z(x'_i)_j), 0) \quad (11)$$

### B. Attack Workflow

Our norm-bounded attack is adjusted from *Projected Gradient Descent (PGD)* [22] to PCSS, and we use NB to denote it. In essence, in each iteration, the attack adds noise to the perturbed point cloud of the previous iteration  $X_T^{i-1}$  to derive  $X_T^i$ , following the goals defined in Equation 1 (targeted) and Equation 4 (non-targeted). Then it clips the changes to  $(-\epsilon, \epsilon)$  on  $X_T^i$ . Random initialization is used to set up  $X_T^0$ . To avoid the imbalance during the update, a sign operator is applied on the gradient. We set an upper bound of iterations as Steps. In each step, we use  $\text{Converge}(\cdot)$  to determine if the adversarial example is satisfactory, based on the attacker's evaluation metrics, e.g., the dropped accuracy.

Algorithm 1 lists the main steps.

Our norm-unbounded attack is adjusted from *Carlini and Wagner (CW)* attack [6], and we use NU to denote it. Algorithm 2 summarizes the workflow, which performs optimization iteratively under the goals defined in Equation 3 (targeted) and 5 (non-targeted), till one termination condition is met. Like NB, we also bound the attack iterations by

---

### Algorithm 1: The pseudo-code of NB for PCSS.

---

**Input:** the original point cloud  $X$ , the ground-truth labels  $Y_{GT}$ , the maximal number of iterations  $Steps$ , the target labels  $Y_T$ , the attack type  $type = \{color, coordinate\}$ , the attack boundary  $\epsilon$ , the target points mask  $\mathcal{T}(\cdot)$  (all points for non-target attack), the targeted points  $T$ , the step size  $\gamma$

**Output:** the adversarial example  $X'$

$X_0 \leftarrow X, r \leftarrow X(type), i \leftarrow 1;$

**while**  $i \leq Steps$  **do**

$X_T^i(type) = \mathcal{T}(r);$

$\mathcal{T}(r) = X_T^i(type) - X_T^{i-1}(type);$

$X_T^i = X_T^{i-1} + \mathcal{T}(r);$

**if** *targeted attack* **then**

$X_T^i = \text{clip}_{(-\epsilon, \epsilon)}(X_T^{i-1} - \gamma \cdot$

$\text{sign}(\nabla_{X_T} \mathcal{L}_T(X_T^{i-1}, Y_T));$

**else if** *non-targeted attack* **then**

$X_T^i = \text{clip}_{(-\epsilon, \epsilon)}(X_T^{i-1} + \gamma \cdot$

$\text{sign}(\nabla_{X_T} \mathcal{L}_{NT}(X_T^{i-1}, Y_{GT}));$

**if** *Converge* **then**

**return**  $X_T^i;$

$i \leftarrow i + 1;$

**end**

**return**  $X_T^i;$

---

Steps. In each step, the gain over the attack is examined by  $\text{Converge}(\cdot)$  as well. If the gain does not increase in 10 steps, the perturbation will add random noise following the uniform distribution in  $(0, 1)$ . When the adversarial example is invalid, e.g.,  $c_i \notin [0, 1]^3$ , a new noise will replace the previous one.

When the attacker chooses to perturb the coordinates, we select a set of most impactful points and only perturb them, such that the  $L_0$  criteria can be met. Especially, in each iteration  $i$ , we assume the points allowed to be perturbed is  $X_i \subseteq X_T$ . After perturbation, the  $n$  least impactful points are selected by the function  $\text{MinImp}(X_i, n)$ , and the point

---

**Algorithm 2:** The pseudo-code of NU for PCSS.

---

**Input:** the original point cloud  $X$ , the ground-truth labels  $Y_{GT}$ , the maximal number of iterations  $Steps$ , the target labels  $Y_T$ , the attack type  $type = \{color, coordinate\}$ , the mask  $\mathcal{T}(\cdot)$ , the targeted points  $T$ , the top  $\alpha$  nearest neighbors, the learning rate  $lr$ , the constant  $\lambda_1, \lambda_2$

**Output:** the adversarial example  $X'$

$X_0 \leftarrow X, r \leftarrow X(type), i \leftarrow 1;$

$w = \tanh^{-1}(2 \cdot \mathcal{T}(r) - 1);$

**while**  $i \leq Steps$  **do**

$X_T^i(type) = \frac{1}{2}\tanh(w) + 1;$

$r = X_T^i(type) - X_T^{i-1}(type);$

$X_T^i = X_T^{i-1} + r;$

$dist = \mathcal{D}(r);$

$smooth = \mathcal{S}(X_T^i, \alpha);$

**if** targeted attack **then**

$loss = \mathcal{L}_T(X_T^i, Y_T);$

**else if** non-targeted attack **then**

$loss = \mathcal{L}_{NT}(X_T^i, Y_{GT});$

$gain_i = dist + \lambda_1 \cdot loss + \lambda_2 \cdot smooth;$

$r = Update(gain_i, lr);$

**if** Converge **then**

$\mathcal{T}(X') = \mathcal{T}X_0 + \mathcal{T}r;$

**return**  $X'$ ;

**else if**  $(i \% (int(Steps * 0.01))) == 0$  &

$(gain_i \geq gain_{i-1})$  **then**

$r = r + \text{uniform noise};$

$i \leftarrow i + 1;$

**end**

$\mathcal{T}(X') = \mathcal{T}X_0 + \mathcal{T}r;$

**return**  $X'$ ;

---

cloud is restored. The next iteration  $i + 1$ , the perturbation will be only executed on  $X_{i+1} = X_i \setminus \text{MinImp}(X_i, n)$ . When the remaining points that can be perturbed are less than 10% after a number of iterations, the point cloud will be perturbed without restoration. The equation below shows how the  $n$  points are selected.

$$\text{MinImp}(X_T^i, n) = \arg \min_n g_n \cdot r_n \quad (12)$$

where  $g_N$  is the gradient and  $r_N$  means the perturbation value.

Noticeably, though our attacks are adjusted from PGD and CW, notable changes exist. For instance, our NB does not use the original cross entropy loss directly and our NU adds a new smoothness penalty.

In Section V-A, the hyper-parameter values used for evaluation for both NB and NU attacks are described.

## V. EVALUATION

In this section, we report our evaluation results on various attack settings, target models, and datasets. Each experiment is conducted to answer one or few research questions (RQ) and the findings are highlighted in the end.

### A. Experiment Settings

**Target Models.** We use the pre-trained PointNet++ [29], ResGCN-28 under the DeepGCN family [16], and RandLA-Net [12] as the target models to evaluate COLPER, mainly because their codes and pre-trained models are publicly available<sup>123</sup>, and they represent different directions in the point cloud domain. In Section II, we give an overview about their designs. Below, we elaborate on their details.

PointNet++ consists of 4 abstraction layers and 4 feature propagation layers with 1 voter number for its multi-angle voting. The overall point accuracy and average Intersection-over-Union (aIoU) of the pre-trained PointNet++ on the indoor dataset S3DIS are 82.65% and 70.71% respectively, as reported in its GitHub repo. ResGCN-28 uses dynamically dilated  $k$ -NN and residual graph connections, and the pre-trained model configures  $k$  to 16. It has 64 filters and 28 blocks with 0.3 drop-out rate and 0.2 stochastic epsilon for GCN. The accuracy and aIoU of the pre-trained ResGCN-28 model on S3DIS are 85.9% and 79.72%, as reported in its GitHub repo. The pre-trained RandLA-Net downsamples large point clouds. Its accuracy and mIoU are 88.0% and 82.0% on S3DIS, and 94.8% and 77.4% on Semantic3D.

**Dataset.** We evaluate the attacks on two large-scale 3D datasets: an indoor dataset S3DIS [1] and an outdoor dataset Semantic3D [11]. They have been extensively used as the benchmark for PCSS. The S3DIS dataset is composed of 3D point clouds with color channels, which were collected at 6 areas in 3 different buildings with 13 class labels. Each point cloud contains 4,096 points, and each point has 9 features. The point cloud data could be pre-processed differently by their segmentation models. As for PointNet++, each point cloud is segmented into several parts, and the coordinate and color are normalized to  $[0, 3]$  and  $[0, 1]$  by themselves. As for ResGCN-28, the coordinate is normalized to  $[-1, 1]$  while the color feature is normalized to  $[0, 1]$  by itself. RandLA-Net regenerates the point clouds with 40,960 points by randomly duplicating and selecting the points. The color feature is also normalized to  $[0, 1]$  by itself.

For the non-targeted attack on S3DIS, we evaluate against the three models with the point clouds of Area 5, of which 198,220 point clouds (78,649,818 points) are included [1]. For the targeted attack, we selected the 100 point clouds in Office 33 of Area 5 when evaluating against PointNet++ and ResGCN-28. As RandLA-Net has different requirements of the point number, for each class (e.g., table), we randomly selected 100 point clouds in Area 5 which at least contains 500 points in the class.

The Semantic3D dataset contains 30 point clouds including coordinates, color channels, and intensity in 8 classes. Each point cloud has over  $10^8$  points to compose a  $160 \times 240 \times 30 m^3$  area. PointNet++ and ResGCN-28 are not designed to

<sup>1</sup>PointNet++: [https://github.com/yanx27/Pointnet\\_Pointnet2\\_pytorch](https://github.com/yanx27/Pointnet_Pointnet2_pytorch)

<sup>2</sup>ResGCN-28: [https://github.com/lightaime/deep\\_gcns\\_torch](https://github.com/lightaime/deep_gcns_torch)

<sup>3</sup>RandLA-Net: <https://github.com/QingyongHu/RandLA-Net>

handle such big point clouds, so we evaluate against RandLA-Net for both the non-targeted and the targeted attack.

**Evaluation Metrics.** We use the drop of accuracy and aIoU as the indicators of the attack’s effectiveness. On a point cloud, accuracy and aIoU are defined as follows: assuming the number of all points and correctly classified points are  $N$  and  $TP$ , accuracy equals to  $\frac{TP}{N}$ . For a class  $i$ , IoU is defined as  $\frac{TP_i}{FN_i+FP_i+TP_i}$ , where  $FN_i$ ,  $FP_i$ ,  $TP_i$  are the number of false negatives, false positives and true positives for the class-related points. Below, we will primarily show the accuracy and aIoU averaged over point clouds.

For the targeted attack, the drop of accuracy and aIoU only measure whether the classification results are changed, but they neglect whether the predictions are misled toward the target classes. Therefore, we define another metric, *point success rate (PSR)*, as the ratio of *points* that are correctly perturbed over all the attacked points in  $X_T$ . When an adversarial sample needs to follow certain constraints to be considered as successful, we use another metric, *sample success rate (SSR)*, to measure the ratio of the perturbed *samples* that meet the criteria. Besides measuring the success rate of attacks, we are also interested in whether the segmentation results of points outside of  $X_T$  are changed, so we compute the accuracy and aIoU on the subset of these points separately, and call the metrics “*out-of-band*” (*OOB*) accuracy and aIoU. From the attacker’s perspective, the drop of OOB accuracy and aIoU should be as low as possible.

**Attack Hyper-parameters.** We set *Steps* to 1,000 for NB and NU. Both  $\lambda_1$  and  $\lambda_2$  used by the adversarial loss are set to 1 based on empirical analysis. The step size ( $\gamma$ ) of NB is 0.01 while the Adam optimizer of NU with 0.01 learning rate ( $lr$ ) is used. The nearest neighbor  $\alpha$  for Equation 9 is set to 10. The batch sizes of are set to 8 when attacking PointNet++ while to 1 when attacking ResGCN-28 and RandLA-Net. For the targeted attack, the adversarial example is considered satisfactory when PSR is above 95%. For the non-targeted attack, we examine whether the accuracy is dropped below 7.6% (*i.e.*, 1/13, 13 classes) for S3IDS and 12.5% (*i.e.*, 1/8) for Semantic3D, which means the model’s prediction is the same as random guessing. When coordinate is attacked,  $n$  least impactful points should be selected in each iteration, and we set  $n$  to 100 during the experiment.

**Experiment Platform.** We run the experiments on a workstation that has an AMD Ryzen Threadripper 3970X 32-Core Processor and 252 GB CPU memory with 2 NVIDIA GeForce RTX 3090. Our attacks run on PyTorch 1.7.1 for the pre-trained PointNet++ and ResGCN-28, and Tensorflow 1.15 for the pre-trained RandLA-Net.

### B. Evaluation on the Attacked Fields

**RQ1:** Which fields are more vulnerable, color or coordinate?

As described in Section II-B, the prior attacks against point cloud objection recognition and semantic segmentation all perturbed the coordinate field, leaving other fields like color feature unexplored. Hence, we first assess how the

TABLE II  
THE NB AND NU RESULTS OF THE  $L_0$  NON-TARGETED ATTACK ON RESGCN-28.

Method	Field	Accuracy (%)	aIoU (%)	SSR (%)
NB	Color	21.99	22.70	44.84
NB	Coordinate	21.80	21.22	4.12
NU	Color	6.84	3.55	81.17
NU	Coordinate	18.11	9.96	11.11

attacked fields impact the attack effectiveness. The experiment is conducted on the S3IDS dataset and the result of non-targeted attack is shown, as the targeted attack follows a similar trend.

Due to that the range of coordinates varies by PCSS models,  $L_2$  distance is unsuitable to measure perturbation, as explained in Section IV. Hence, we use  $L_0$  distance for the coordinate-based attack. For a fair comparison, we also change the  $L_2$  distance used by a feature-based attack to  $L_0$ . We define SSR in this experiment as the ratio of the adversarial samples that perturb less than 10% points (explained in Section IV-B) of a point cloud and drop the segmentation accuracy below 7.69% (random guessing).

Our results in Table II shows that when ResGCN-28 is the target model, SSR is significantly higher for color-based attack than coordinate-based attack (81.17% versus 11.11% for NU and 44.84% versus 4.12% for NB). The average accuracy and aIoU (counted together from both successful and unsuccessful samples) under NU for color-based attack are also much lower than coordinate-based attack. On PointNet++, we found that coordinate-based attack cannot even meet the attack criteria of finding less than 10% points, while color-based attack not only meets the attack criteria but also drops the segmentation accuracy to 17.23% under NB and 12.20% under NU. We skip RandLA-Net because it handles coordinates in a very different way from PointNet++ and ResGCN-28.

Overall, our result suggests PCSS models have a much better capability in handling abnormal coordinates than abnormal features. Given that perturbing point color is much more effective than perturbing point coordinates, for the following experiments, all attacks are conducted under color-based perturbation, and we switch the distance back to the default  $L_2$ .

**RQ1 Finding:** The color features are more vulnerable than point coordinates under perturbation.

### C. Evaluation on Non-targeted Attack

**RQ2:** Which attack method is more effective under non-targeted attack?

**RQ3:** Does attack effectiveness varies by the target model?

In this subsection, we conduct experiments under the non-target attack setting, focusing on the attack effectiveness under different methods and target models. We use S3IDS as the dataset. For the attack methods, in addition to NU and NB, we also implement another method that adds random noises to the color channels, as a baseline to compare against.

TABLE III

NON-TARGETED ATTACK AGAINST POINTNET++, RESGCN-28, AND RANDLA-NET ON S3DIS. THE COLOR FEATURE IS ATTACKED AND  $L_2$  DISTANCE IS USED.

Case		Random Noise			NU			NB		
		$L_2$	Accuracy (%)	aIoU (%)	$L_2$	Accuracy (%)	aIoU (%)	$L_2$	Accuracy (%)	aIoU (%)
PointNet++	Best	2.68	14.51	14.26	2.68	4.91	2.31	15.51	5.71	5.19
	Avg.	18.19	77.26(5.39↓)	70.02(0.69↓)	<b>18.27</b>	<b>7.86</b> (74.79↓)	<b>8.85</b> (61.86↓)	18.27	19.11(63.54↓)	16.10(54.61↓)
	Worst	30.02	100	100	30.03	20.33	59.27	22.01	56.71	42.37
ResGCN-28	Best	1.29	7.79	4.11	1.29	0.31	0.16	5.05	0.0	0.0
	Avg.	4.30	82.36(3.54↓)	73.17(6.55↓)	<b>4.30</b>	<b>6.75</b> (79.15↓)	<b>3.49</b> (76.23↓)	6.51	42.16(43.74↓)	30.13(49.59↓)
	Worst	9.81	100	100	9.81	18.34	10.10	7.96	99.85	99.70
RandLA-Net	Best	6.65	34.07	12.56	6.65	6.13	0.92	0.33	18.52	13.62
	Avg.	17.06	78.01(6.24↓)	44.82(6.6↓)	<b>17.06</b>	<b>7.45</b> (76.75↓)	<b>2.96</b> (48.45↓)	16.83	59.60(24.65↓)	31.15(20.26↓)
	Worst	54.62	97.18	70.08	54.62	7.69	8.33	17.00	85.88	66.18

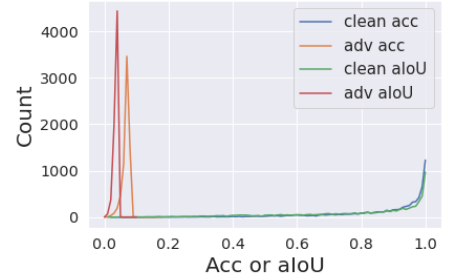
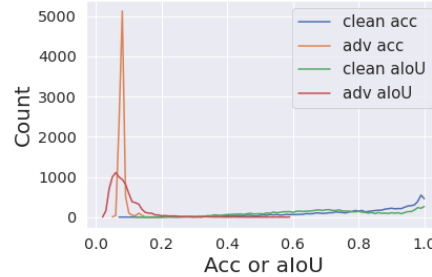
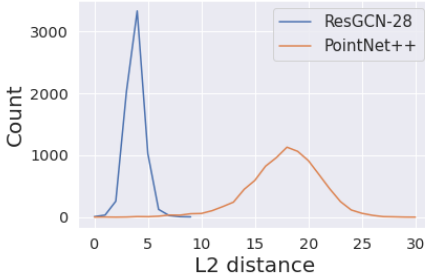


Fig. 3. The  $L_2$  distance distribution on PointNet++ and ResGCN-28.

Fig. 4. The accuracy and aIoU distribution on PointNet++.

Fig. 5. The accuracy and aIoU distribution on ResGCN-28.

In Table III, we show accuracy and aIoU across the tested point clouds (“best” and “worst” show the examples most vulnerable and robust against the attack). We also show the  $L_2$  distance between the original point cloud and the perturbed version. It turns out NU and NB both can significantly reduce accuracy and aIoU. For example, NU *drops the average accuracy of PointNet++, ResGCN-28, and RandLA-Net from 82.65% to 7.86%, 85.90% to 6.75%, and 87.2% to 7.45% separately*. aIoU is also dropped in a similar trend, and the average drop rate ranges from 48.45% to 76.23% under NU, and from 20.26 to 54.61% under NB. NU performs much better for the worst-case scenario, i.e., the most difficult sample: e.g., when ResGCN-28 is attacked, NU is able to drop the accuracy on the most difficult sample to 18.34%, but NB has nearly 0 impacts on the accuracy (99.85%).

Regarding the perturbation distance, we found NU generates the adversarial examples under smaller or equal distance in the best-case scenario and average scenarios for PointNet++ and ResGCN-28, but the distance becomes larger for RandLA-Net (e.g., 17.06 compared to 16.83 for the average). For the worst-case scenario, NU has to add much larger noises to drop accuracy and aIoU.

Regarding the baseline method, we found its effectiveness is quite limited, with the dropping of average accuracy and aIoU ranging from 3.54% to 6.24% and 0.69% to 6.6% respectively. The result suggests PCSS models are robust against random noises and carrying out a successful attack is non-trivial.

Regarding the impact of the target model on the attack effectiveness, we found NU is similarly effective against Point-

Net++, ResGCN-28, and RandLA-Net, but NB is much more effective against PointNet++ than ResGCN-28 and RandLA-Net. Hence, we suggest that NU should be used if the attacker prefers effectiveness, or finding better adversarial examples. In the meantime, NU usually takes a longer time to execute due to the longer time to reach the converge requirement. Our performance evaluation shows that NB is around 5X faster than NU on average.

To gain a better understanding of NU at the sample level, in Figure 3, Figure 4 and Figure 5, we show the  $L_2$  distance, accuracy and aIoU of each point cloud and draw their distributions after the attack on PointNet++ and ResGCN-28. We do not consider RandLA-Net in the analysis due to its specialized point sampling during data pre-processing. The y-axis of each figure is the number of point clouds. “clean” and “adv” mean the results before and after our attack. We found that the accuracy and aIoU after the attack are *consistently below 20%*, showing NU is effective across samples. For the distribution on ResGCN-28 (Figure 5), we found NU is similarly effective across samples but the perturbation distance is much smaller compared to PointNet++, ranging from 3.5 to 6.5 (PointNet++ has the range of 11 to 25).

**RQ2 Finding:** Under non-targeted attack, NU is more effective than NB, especially for the most difficult point cloud samples.

**RQ3 Finding:** All tested models are similarly vulnerable under NU, but PointNet++ is much more vulnerable under NB.



#### D. Evaluation on Targeted Attack

**RQ4:** Which attack method is more effective under targeted attack?

**RQ5:** How does the object class impact the attack effectiveness?

Following the evaluation of the non-targeted attack, here we evaluate the targeted attack under NU and NB. We used Area 5 of S3IDS for evaluation, which contains objects under 13 classes, and we perturb the points from 6 classes, including window (label=5), door (label=6), table (label=7), chair (label=8), bookcase (label=10), and board (label=11), because the quantity of points of each class is not too small. We set the target class as wall (label=2).

Table IV shows the results for the 6 objects under NU. It turns out *PSR can be over 90%* for window, door, bookcase, and board, against all targeted models. However, PSR is much lower for table and chair. We speculate the reason is that table and chair have more complex shapes, so changing the class labels on these objects is more difficult. In the meantime, the drop in the accuracy of the OOB points is moderate, mostly within 10%, which suggests NU is able to confine the changes to the selected objects.

Table V shows the results under NB. Similar to the trend of the non-targeted attack, NB performs worse than NU, i.e., lower PSR for every perturbed object. Regarding the impact of objects, we also found PSR is higher when less complex objects like window, door, bookcase and board are perturbed, but table and chair see much lower PSR than NU, e.g., under 10% for PointNet++ and ResGCN-28. Moreover, NB results in a larger drop of OOB accuracy and aIOU, especially for PointNet++ and ResGCN-28.

Since the design of NB bounds the perturbation distance, we found the  $L_2$  distance of adversarial samples is much smaller than NU in most cases, though it comes at the price of lower PSR.

Regarding the target model, we found it is easier to achieve high PSR when attacking RandLA-Net. For example, even table and chair have over 80% PSR for NU and NB.

**RQ4 Finding:** under targeted attack, NU is also more effective than NB.

**RQ5 Finding:** source class has big impact on the attack effectiveness, as changing the labels on the complex objects is much harder.

#### E. Evaluation on Outdoor Dataset

**RQ6:** Is outdoor scene also vulnerable?

All previous evaluations are carried out on S3IDS, an indoor dataset. Since the outdoor scenes have different properties (e.g., different object classes and larger sizes), we evaluate the attacks against another outdoor dataset, Semantic3D. Only RandLA-Net is attacked because the other two PCSS models cannot handle the scale of point clouds in Semantic3D. We show the result of NU only as it is more effective than NB in previous experiments.

Table VI shows the results of the non-targeted attack. Similar as the attack against S3IDS, NU greatly decreases the accuracy and aIoU comparing to the baseline (random noises) when they target the same  $L_2$  distance: the average accuracy and aIoU drop from 98.25% and 63.26% to 16.00% and 7.70%. The baseline only drops average accuracy and aIoU to 79.30% and 37.22%. We also observe that the result on RandLA-Net has bigger variance by samples: e.g., the accuracy can drop to 0% for the best case, and 90.82% for the worst case.

As for the targeted attack, we manipulate the source points labeled as car (label=8) and try to mislead the model to predict them as man-made terrain (label=1), natural terrain (label=2), high vegetation (label=3) and low vegetation (label=4). From Table VII, PSR is near 95% when vegetation is the target class. Though outdoor scene is expected to be more complex, our result shows targeted attack is still effective.

**RQ6 Finding:** NU is also effective when attacking an outdoor scene, under both the non-targeted and the targeted attack.

#### F. Attack Transferability

**RQ7:** Can the generated adversarial example be applied on another PCSS model?

Existing research has shown an adversarial sample targeting 2D image classification has transferability [27], i.e., that a sample generated against one model is also effective against another model. We are interested in whether our adversarial samples have the same property. To this end, we first evaluate the attack transferability on models with different parameters. We select 400 non-targeted adversarial samples generated by NU on the pre-trained PointNet++, and feed them into another PointNet++ trained by ourselves (the weights and biases are different). The results in Table VIII show the accuracy and aIoU on the 400 samples, and both are less than 40%, suggesting our adversarial sample is transferable under different model parameters.

Then we test transferability across model families: we generate adversarial examples for ResGCN-28 and test if they can fool PointNet++. We do not transfer the attack against RandLA-Net due to its highly different approach of pre-processing. Due to different normalization steps (i.e., the coordinate ranges in  $[-1, 1]$  for ResGCN-28 while  $[0, 3]$  for PointNet++), the adversarial samples do not directly transfer, and we perform an extra step to map the attacked fields to the same range. We compute the accuracy and aIoU in the two settings, and the results suggest our samples is also transferrable (Table VIII).

**RQ7 Finding:** The adversarial example is transferable under different model parameters and across model families.

#### G. Visualization of Adversarial Examples

In this subsection, we visualize the adversarial examples generated under color-based NU. For each sample, we show

TABLE IV

THE RESULTS OF THE TARGETED ATTACK OF NU ON WINDOW (LABEL=5), DOOR (LABEL=6), TABLE (LABEL=7), CHAIR (LABEL=8), BOOKCASE (LABEL=10), BOARD (LABEL=11).

Model	Source Class	$L_2$	PSR (%)	OOB Acc/Acc (%)	OOB aIoU/aIoU (%)
PointNet++	window	7.67	<b>93.92</b>	53.76 / 77.67	46.59 / 60.77
	door	5.39	<b>93.11</b>	58.54 / 62.00	45.37 / 49.24
	table	10.55	37.70	79.48 / 86.26	56.04 / 69.09
	chair	6.69	17.63	86.09 / 90.65	62.91 / 73.19
	bookcase	15.26	<b>93.25</b>	52.73 / 68.43	49.63 / 57.88
	board	5.28	<b>93.16</b>	80.47 / 93.97	60.99 / 74.27
ResGCN-28	window	14.57	<b>95.44</b>	70.88 / 71.21	39.57 / 58.67
	door	12.17	<b>94.71</b>	77.96 / 84.62	65.11 / 76.75
	table	9.29	66.43	81.81 / 91.66	49.08 / 84.80
	chair	12.62	51.63	82.22 / 83.84	63.39 / 75.59
	bookcase	16.01	<b>90.48</b>	65.10 / 68.43	55.56 / 56.52
	board	9.69	<b>96.08</b>	78.37 / 88.85	56.58 / 66.43
RandLA-Net	window	3.76	<b>95.13</b>	83.98 / 84.41	50.39 / 51.03
	door	2.79	<b>95.23</b>	88.42 / 88.78	49.52 / 51.12
	table	11.82	83.10	83.11 / 83.98	45.01 / 50.58
	chair	9.06	85.98	82.78 / 82.94	47.50 / 47.94
	bookcase	8.55	<b>95.05</b>	84.02 / 84.71	50.07 / 51.27
	board	2.37	<b>94.29</b>	84.80 / 85.57	52.22 / 54.06

TABLE V

THE RESULTS OF THE TARGETED ATTACK OF NB ON WINDOW (LABEL=5), DOOR (LABEL=6), TABLE (LABEL=7), CHAIR (LABEL=8), BOOKCASE (LABEL=10), BOARD (LABEL=11).

Model	Source Class	$L_2$	PSR (%)	OOB Acc/Acc (%)	OOB aIoU/aIoU (%)
PointNet++	window	5.44	81.12	34.55 / 81.66	32.53 / 70.31
	door	3.78	42.85	88.72 / 94.67	52.42 / 66.60
	table	5.78	3.84	60.71 / 85.67	52.42 / 67.20
	chair	3.02	1.04	65.33 / 85.24	42.25 / 67.20
	bookcase	5.26	42.22	47.60 / 71.44	41.24 / 61.49
	board	6.85	70.58	74.55 / 89.23	48.37 / 63.41
ResGCN-28	window	4.25	65.80	44.60 / 80.90	42.53 / 69.31
	door	4.16	26.27	65.76 / 88.03	65.72 / 79.88
	table	4.23	1.24	63.89 / 88.85	61.24 / 81.73
	chair	4.35	0.90	62.00 / 93.02	59.73 / 88.02
	bookcase	5.87	7.35	45.46 / 83.72	58.00 / 73.93
	board	3.83	26.20	67.59 / 91.15	64.87 / 84.67
RandLA-Net	window	3.86	82.42	81.50 / 84.42	44.93 / 50.48
	door	3.97	83.05	81.82 / 84.57	44.28 / 50.18
	table	4.42	80.95	80.85 / 84.55	44.14 / 51.20
	chair	4.19	83.59	81.55 / 83.96	45.31 / 50.95
	bookcase	3.99	91.87	82.88 / 84.66	47.38 / 51.28
	board	2.83	93.95	86.45 / 86.74	52.73 / 56.69

the original and perturbed scenes and their segmentation results.

First, we show the scenes in S3IDS under non-targeted attack and PointNet++ is the target model. We choose different types of scenes like the conference room, hallway, and lobby. From Figure 6, we can see the small perturbation generated by our attack leads to prominent changes in the segmentation results.

Next, we show an example about the targeted attack in Figure 7. We set PointNet++ as the target model, and board as the source class. Since most of its points are classified as wall after the attack, our attack could make the board nearly “disappear” from the view of the segmentation model.

When multiple source classes are perturbed, our attack is demonstrated effective as well. One example is visualized in Figure 8. We consider table (label=7), chair (label=8), and bookcase (label=10) as the source classes to be changed, and

PointNet++ as the segmentation model. The result shows they are all mis-classified as wall by the segmentation model.

Finally, we show an example about an outdoor scene under Semantic3D in Figure 9, under non-targeted attack, with RandLA-Net as the targeted model. The visualized result also suggests seemingly small perturbations can drastically change the segmentation results.

## VI. DISCUSSION

### A. Defenses

To mitigate the threats from the proposed adversarial attacks, gradient obfuscation, adversarial training, and anomaly detection can be tested on PCSS. These ideas have been initially examined on 2D image classification and were recently migrated to 3D point cloud object recognition. For gradient obfuscation, DUP-Net [51] includes a denoiser layer and upsampler network structure. GvG-PointNet++ [8] introduces

TABLE VI  
THE RESULTS OF THE NON-TARGETED ATTACK FROM RANDLA-NET ON SEMANTIC3D.

Case	Random Noise			NU		
	L <sub>2</sub>	Accuracy (%)	aIoU (%)	L <sub>2</sub>	Accuracy (%)	aIoU (%)
Best	19.31	0.00	0.00	19.31	0.00	0.00
Average	25.84	79.30(18.95↓)	37.22(26.04 ↓)	<b>25.84</b>	<b>16.00(82.25↓)</b>	<b>7.70(55.56%↓)</b>
Worst	280.79	100.0	100.0	280.79	90.82	25.42

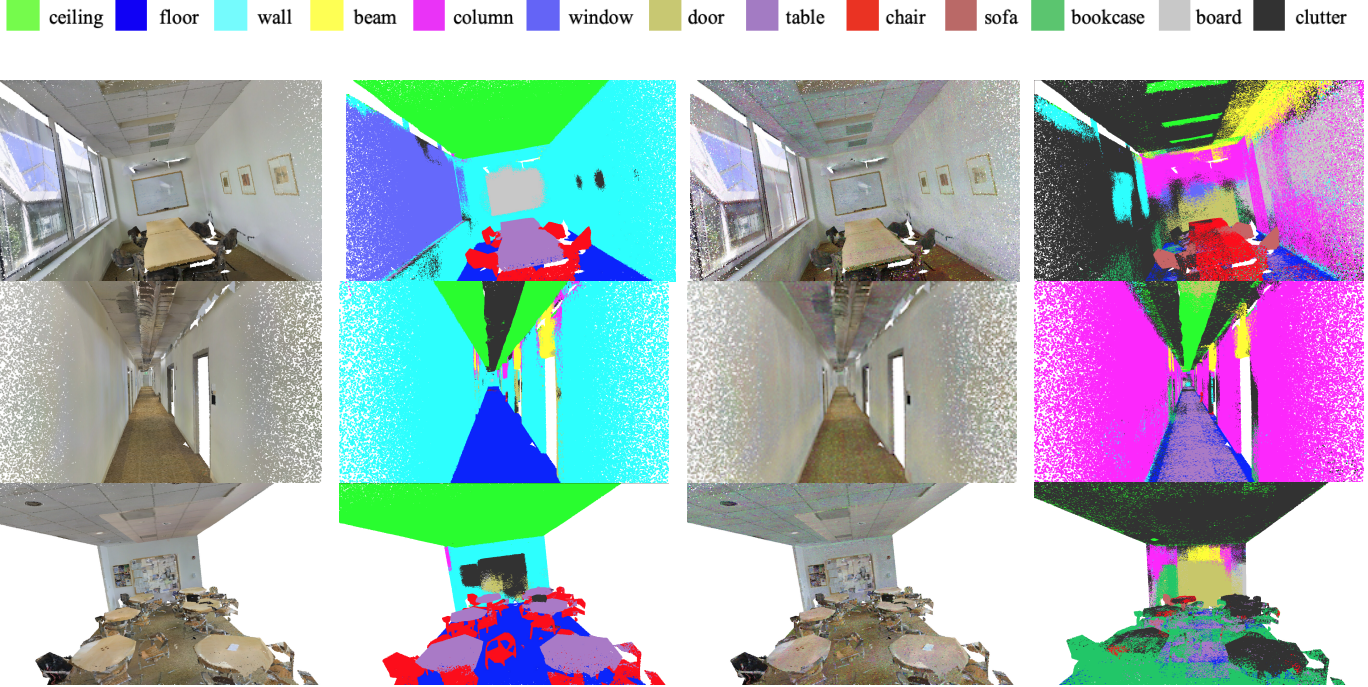


Fig. 6. The non-targeted attack with Conference room 1 (first row), Hallway 2 (second row), Lobby 1 (third row) of Area 5 in S3DIS. The first to fourth columns show the original scene, the original segmentation results, perturbed scene and perturbed segmentation results.

TABLE VII  
THE RESULTS OF THE TARGETED ATTACK AGAINST RANDLA-NET ON SEMANTIC3D. CAR (LABEL=8) IS PERTURBED TO MAN-MADE TERRAIN (LABEL=1), NATURAL TERRAIN (LABEL=2), HIGH VEGETATION (LABEL=3), LOW VEGETATION (LABEL=4).

Target Class	L <sub>2</sub>	PSR	OOB Acc/Acc(%)	OOB aIoU/aIoU(%)
Man-made terrain	10.41	85.30	73.03 / 73.64	30.74 / 33.56
Natural terrain	5.61	73.96	84.76 / 84.89	46.63 / 48.19
High vegetation	3.61	<b>94.26</b>	97.95 / 97.99	58.86 / 61.51
Low vegetation	3.60	<b>94.86</b>	74.18 / 74.70	39.57 / 42.52

gather vectors in the points clouds. However, these approaches might still be vulnerable, due to the inherent limitation of gradient obfuscation under the white-box adaptive attacks [33]. Recently, Li et al. [18] proposed implicit gradients, which could lead the attackers to the wrong updating directions, to replace obfuscated gradients. Whether this approach is robust under the adaptive attacker needs to be further examined. For adversarial training, DeepSym [33] uses a sorting-based pooling operation to overcome the issues caused by the default symmetric function. However, the robustness comes with the

TABLE VIII  
THE UPPER ROW SHOWS THE RESULTS OF ATTACK TRANSFERABILITY ON POINTNET++. THE LOWER ROW DISPLAYS THE RESULTS FROM TRANSFERRING RESGCN-28 ADVERSARIAL SAMPLES TO POINTNET++.

PCSS Model	Accuracy (%)	aIoU (%)
PointNet++ (Pre-trained)	7.24	9.44
PointNet++ (Self-trained)	34.35	31.39
ResGCN-28	7.11	3.68
PointNet++	39.01	25.30

cost of high training overhead. For anomaly detection, [45] measured the statistics of the perturbed outputs to detect the adversarial example. Yet, none of the prior works were tested on PCSS and it is unclear if they are effective for the model architecture other than CNN, e.g., GCN. As future work, we plan to evaluate the defenses on PCSS and adjust them when necessary.

### B. Limitations

(1) Currently we select three representative PCSS models and the robustness of them are analyzed thoughtfully on two datasets. Though we are able to cover different model families (e.g., CNN and GCN) and different real-world settings (indoor

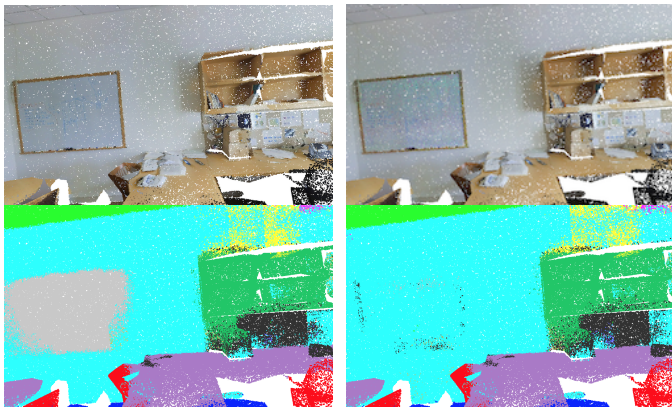


Fig. 7. The targeted attack with Office 33 of Area 5 in S3DIS. The upper left, upper right, lower left, and lower right show the original scene, the perturbed scene, and the segmentation results of the original and perturbed scene.

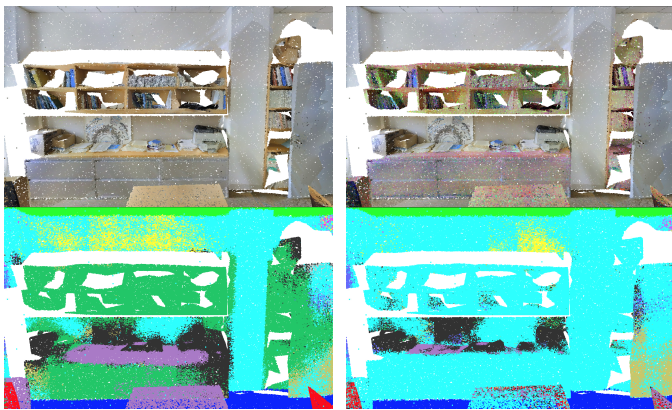


Fig. 8. The targeted attack against multiple source classes in Office 33 of Area 5 in S3DIS. Table, chair and bookcase are all misclassified as wall after the attack.

and outdoor), admittedly we could extend the study scope by including more models and datasets. (2) For RandLA-Net, we did not implement the coordinate-based attack as its point sampling mechanism makes it more difficult to locate the points for attack. How to derive robust attack that circumvent such mechanisms could be an interesting topic to explore. (3) The focus of this study is to examine the robustness of different PCSS models and settings. Unlike [52], we did not convert the perturbation on the point cloud into the changes in the physical world, e.g., using irregular objects or stickers. Yet, our study could provide guidance in designing physically realizable adversarial examples.

## VII. CONCLUSION

In this work, we present the first comparative study of adversarial attacks on 3D point cloud semantic segmentation (PCSS). We systematically formulate the attacker’s objectives under the targeted attack and the non-targeted attack, and develop two attack methods based on norm-bounded NB attack and norm-unbounded NU attack. In addition to the point coordinates that are exploited by all existing adversarial

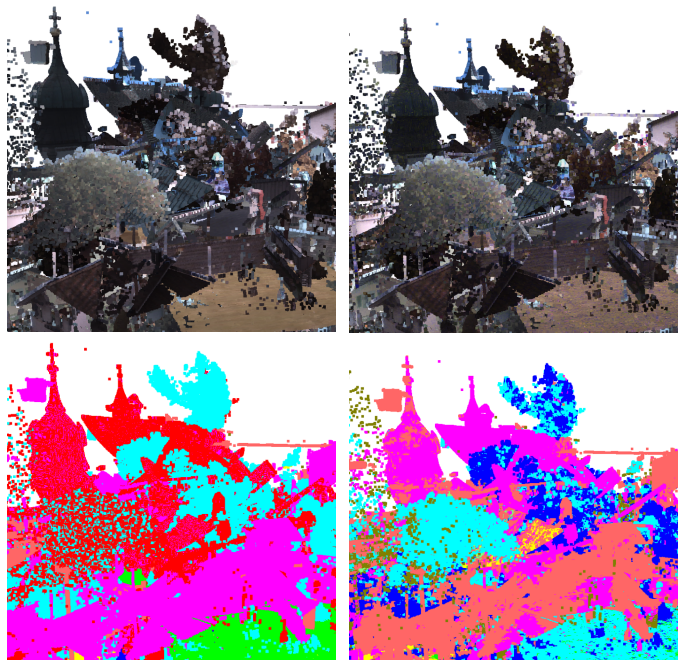


Fig. 9. An example of the non-targeted attack against Semantic3D.

attacks, we consider point features to be perturbed. We examine these attack combinations on an indoor dataset S3DIS and an outdoor dataset Semantic3D dataset, to examine the impact of each attack option. To highlight our evaluation result, we found feature-based attack, especially color-based attack, is more effective than coordinate-based attack. Norm-unbounded NU attack is more effective, driving down the accuracy and aIoU by a big margin, and the result is consistent across scenes and the targeted models. For the targeted attack, we observe the prominent differences between objects, and how to make the targeted attack effective across different classes warrant future research. All targeted models, including PointNet++, ResGCN-28 and RandLA-Net, are vulnerable, and the adversarial examples are transferrable. We hope with this study, more attention can be paid to make PCSS models more robust, and our study provides guidance in developing robust PCSS models.

## REFERENCES

- [1] Iro Armeni, Sasha Sax, Amir R Zamir, and Silvio Savarese. Joint 2d-3d-semantic data for indoor scene understanding. *arXiv preprint arXiv:1702.01105*, 2017.
- [2] Iro Armeni, Ozan Sener, Amir R Zamir, Helen Jiang, Ioannis Brilakis, Martin Fischer, and Silvio Savarese. 3d semantic parsing of large-scale indoor spaces. In *Proceedings of the IEEE Conference on Computer Vision and Pattern Recognition*, pages 1534–1543, 2016.
- [3] Anurag Arnab, Ondrej Miksik, and Philip HS Torr. On the robustness of semantic segmentation models to adversarial attacks. In *Proceedings of the IEEE Conference on Computer Vision and Pattern Recognition*, pages 888–897, 2018.
- [4] Jens Behley, Martin Garbade, Andres Milioto, Jan Quenzel, Sven Behnke, Cyrill Stachniss, and Jurgen Gall. Semantickitti: A dataset for semantic scene understanding of lidar sequences. In *Proceedings of the IEEE/CVF International Conference on Computer Vision*, pages 9297–9307, 2019.

- [5] Yulong Cao, Chaowei Xiao, Dawei Yang, Jing Fang, Ruigang Yang, Mingyan Liu, and Bo Li. Adversarial objects against lidar-based autonomous driving systems. *arXiv preprint arXiv:1907.05418*, 2019.
- [6] Nicholas Carlini and David Wagner. Towards evaluating the robustness of neural networks. In *2017 IEEE symposium on security and privacy (sp)*, pages 39–57. IEEE, 2017.
- [7] Angel X Chang, Thomas Funkhouser, Leonidas Guibas, Pat Hanrahan, Qixing Huang, Zimo Li, Silvio Savarese, Manolis Savva, Shuran Song, Hao Su, et al. Shapenet: An information-rich 3d model repository. *arXiv preprint arXiv:1512.03012*, 2015.
- [8] Xiaoyi Dong, Dongdong Chen, Hang Zhou, Gang Hua, Weiming Zhang, and Nenghai Yu. Self-robust 3d point recognition via gather-vector guidance. In *Proceedings of the IEEE/CVF Conference on Computer Vision and Pattern Recognition*, pages 11516–11524, 2020.
- [9] Kevin Eykholt, Ivan Evtimov, Earlene Fernandes, Bo Li, Amir Rahmati, Chaowei Xiao, Atul Prakash, Tadayoshi Kohno, and Dawn Song. Robust physical-world attacks on deep learning visual classification. In *Proceedings of the IEEE Conference on Computer Vision and Pattern Recognition*, pages 1625–1634, 2018.
- [10] Ian J Goodfellow, Jonathon Shlens, and Christian Szegedy. Explaining and harnessing adversarial examples. *arXiv preprint arXiv:1412.6572*, 2014.
- [11] Timo Hackel, Nikolay Savinov, Lubor Ladicky, Jan D Wegner, Konrad Schindler, and Marc Pollefeys. Semantic3d. net: A new large-scale point cloud classification benchmark. *arXiv preprint arXiv:1704.03847*, 2017.
- [12] Qingyong Hu, Bo Yang, Linhai Xie, Stefano Rosa, Yulan Guo, Zhihua Wang, Niki Trigoni, and Andrew Markham. Randla-net: Efficient semantic segmentation of large-scale point clouds. In *Proceedings of the IEEE/CVF Conference on Computer Vision and Pattern Recognition*, pages 11108–11117, 2020.
- [13] Qidong Huang, Xiaoyi Dong, Dongdong Chen, Hang Zhou, Weiming Zhang, and Nenghai Yu. Shape-invariant 3d adversarial point clouds. In *Proceedings of the IEEE/CVF Conference on Computer Vision and Pattern Recognition*, pages 15335–15344, 2022.
- [14] Alexey Kurakin, Ian Goodfellow, and Samy Bengio. Adversarial machine learning at scale. *arXiv preprint arXiv:1611.01236*, 2016.
- [15] Loic Landrieu and Simonovsky Martin. Large-scale Point Cloud Semantic Segmentation with Superpoint Graphs. In *2018 IEEE Conference on Computer Vision and Pattern Recognition (CVPR 2018)*, Salt Lake City, United States, June 2018.
- [16] Guohao Li, Matthias Muller, Ali Thabet, and Bernard Ghanem. Deepgcns: Can gcns go as deep as cnns? In *Proceedings of the IEEE International Conference on Computer Vision*, pages 9267–9276, 2019.
- [17] Jiaxin Li, Ben M Chen, and Gim Hee Lee. So-net: Self-organizing network for point cloud analysis. In *Proceedings of the IEEE conference on computer vision and pattern recognition*, pages 9397–9406, 2018.
- [18] Kaidong Li, Ziming Zhang, Cuncong Zhong, and Guanghui Wang. Robust structured declarative classifiers for 3d point clouds: Defending adversarial attacks with implicit gradients. In *Proceedings of the IEEE/CVF Conference on Computer Vision and Pattern Recognition*, pages 15294–15304, 2022.
- [19] Yangyan Li, Rui Bu, Mingchao Sun, Wei Wu, Xinhan Di, and Baoquan Chen. Pointcnn: Convolution on  $\chi$ -transformed points. In *Proceedings of the 32nd International Conference on Neural Information Processing Systems*, pages 828–838, 2018.
- [20] Binbin Liu, Jinlai Zhang, and Jihong Zhu. Boosting 3d adversarial attacks with attacking on frequency. *IEEE Access*, 10:50974–50984, 2022.
- [21] Daniel Liu, Ronald Yu, and Hao Su. Extending adversarial attacks and defenses to deep 3d point cloud classifiers. In *2019 IEEE International Conference on Image Processing (ICIP)*, pages 2279–2283. IEEE, 2019.
- [22] Aleksander Madry, Aleksandar Makelov, Ludwig Schmidt, Dimitris Tsipras, and Adrian Vladu. Towards deep learning models resistant to adversarial attacks. *arXiv preprint arXiv:1706.06083*, 2017.
- [23] Kirill Mazur and Victor Lempitsky. Cloud transformers. *arXiv preprint arXiv:2007.11679*, 2020.
- [24] Kaichun Mo, Shilin Zhu, Angel X Chang, Li Yi, Subarna Tripathi, Leonidas J Guibas, and Hao Su. Partnet: A large-scale benchmark for fine-grained and hierarchical part-level 3d object understanding. In *Proceedings of the IEEE/CVF conference on computer vision and pattern recognition*, pages 909–918, 2019.
- [25] Krishna Kanth Nakka and Mathieu Salzmann. Indirect local attacks for context-aware semantic segmentation networks. In *European Conference on Computer Vision*, pages 611–628. Springer, 2020.
- [26] Federico Nesti, Giulio Rossolini, Saasha Nair, Alessandro Biondi, and Giorgio Buttazzo. Evaluating the robustness of semantic segmentation for autonomous driving against real-world adversarial patch attacks. In *Proceedings of the IEEE/CVF Winter Conference on Applications of Computer Vision*, pages 2280–2289, 2022.
- [27] Nicolas Papernot, Patrick McDaniel, and Ian Goodfellow. Transferability in machine learning: from phenomena to black-box attacks using adversarial samples. *arXiv preprint arXiv:1605.07277*, 2016.
- [28] Charles R Qi, Hao Su, Kaichun Mo, and Leonidas J Guibas. Pointnet: Deep learning on point sets for 3d classification and segmentation. In *Proceedings of the IEEE conference on computer vision and pattern recognition*, pages 652–660, 2017.
- [29] Charles Ruizhongtai Qi, Li Yi, Hao Su, and Leonidas J Guibas. Pointnet++: Deep hierarchical feature learning on point sets in a metric space. In *Advances in neural information processing systems*, pages 5099–5108, 2017.
- [30] Guocheng Qian, Yuchen Li, Houwen Peng, Jinjie Mai, Hasan Abed Al Kader Hammoud, Mohamed Elhoseiny, and Bernard Ghanem. Pointnext: Revisiting pointnet++ with improved training and scaling strategies. *arXiv preprint arXiv:2206.04670*, 2022.
- [31] Damien Robert, Bruno Vallet, and Loic Landrieu. Learning multi-view aggregation in the wild for large-scale 3d semantic segmentation. In *Proceedings of the IEEE/CVF Conference on Computer Vision and Pattern Recognition*, pages 5575–5584, 2022.
- [32] Dong Wook Shu, Sung Woo Park, and Junseok Kwon. 3d point cloud generative adversarial network based on tree structured graph convolutions. In *Proceedings of the IEEE/CVF International Conference on Computer Vision*, pages 3859–3868, 2019.
- [33] Jiachen Sun, Karl Koenig, Yulong Cao, Qi Alfred Chen, and Z Morley Mao. On the adversarial robustness of 3d point cloud classification. *arXiv preprint arXiv:2011.11922*, 2020.
- [34] Liyao Tang, Yibing Zhan, Zhe Chen, Baosheng Yu, and Dacheng Tao. Contrastive boundary learning for point cloud segmentation. In *Proceedings of the IEEE/CVF Conference on Computer Vision and Pattern Recognition*, pages 8489–8499, 2022.
- [35] Hugues Thomas, Charles R Qi, Jean-Emmanuel Deschaud, Beatriz Marcotequi, François Goulette, and Leonidas J Guibas. Kpconv: Flexible and deformable convolution for point clouds. In *Proceedings of the IEEE/CVF International Conference on Computer Vision*, pages 6411–6420, 2019.
- [36] Tzungyu Tsai, Kaichen Yang, Tsung-Yi Ho, and Yier Jin. Robust adversarial objects against deep learning models. In *Proceedings of the AAAI Conference on Artificial Intelligence*, volume 34, pages 954–962, 2020.
- [37] James Tu, Mengye Ren, Sivabalan Manivasagam, Ming Liang, Bin Yang, Richard Du, Frank Cheng, and Raquel Urtasun. Physically realizable adversarial examples for lidar object detection. In *Proceedings of the IEEE/CVF Conference on Computer Vision and Pattern Recognition*, pages 13716–13725, 2020.
- [38] Mikaela Angelina Uy, Quang-Hieu Pham, Binh-Son Hua, Thanh Nguyen, and Sai-Kit Yeung. Revisiting point cloud classification: A new benchmark dataset and classification model on real-world data. In *Proceedings of the IEEE/CVF international conference on computer vision*, pages 1588–1597, 2019.
- [39] Jiacheng Wei, Guosheng Lin, Kim-Hui Yap, Tzu-Yi Hung, and Lihua Xie. Multi-path region mining for weakly supervised 3d semantic segmentation on point clouds. In *Proceedings of the IEEE/CVF Conference on Computer Vision and Pattern Recognition (CVPR)*, June 2020.
- [40] Matthew Wicker and Marta Kwiatkowska. Robustness of 3d deep learning in an adversarial setting. *CoRR*, abs/1904.00923, 2019.
- [41] Zhirong Wu, Shuran Song, Aditya Khosla, Fisher Yu, Linguang Zhang, Xiaoou Tang, and Jianxiong Xiao. 3d shapenets: A deep representation for volumetric shapes. In *Proceedings of the IEEE conference on computer vision and pattern recognition*, pages 1912–1920, 2015.
- [42] Chong Xiang, Charles R Qi, and Bo Li. Generating 3d adversarial point clouds. *Proc. Computer Vision and Pattern Recognition (CVPR)*, IEEE, 2019.
- [43] Cihang Xie, Jianyu Wang, Zhishuai Zhang, Yuyin Zhou, Lingxi Xie, and Alan Yuille. Adversarial examples for semantic segmentation and object detection. In *Proceedings of the IEEE International Conference on Computer Vision*, pages 1369–1378, 2017.
- [44] Qiangeng Xu, Xudong Sun, Cho-Ying Wu, Panqu Wang, and Ulrich Neumann. Grid-gcn for fast and scalable point cloud learning. In

- Proceedings of the IEEE/CVF Conference on Computer Vision and Pattern Recognition*, pages 5661–5670, 2020.
- [45] Jiancheng Yang, Qiang Zhang, Rongyao Fang, Bingbing Ni, Jinxian Liu, and Qi Tian. Adversarial attack and defense on point sets. *arXiv preprint arXiv:1902.10899*, 2019.
- [46] Hengshuang Zhao, Li Jiang, Jiaya Jia, Philip HS Torr, and Vladlen Koltun. Point transformer. In *Proceedings of the IEEE/CVF International Conference on Computer Vision*, pages 16259–16268, 2021.
- [47] Yue Zhao, Hong Zhu, Ruigang Liang, Qintao Shen, Shengzhi Zhang, and Kai Chen. Seeing isn't believing: Towards more robust adversarial attack against real world object detectors. In *Proceedings of the 2019 ACM SIGSAC Conference on Computer and Communications Security*, pages 1989–2004, 2019.
- [48] Tianhang Zheng, Changyou Chen, Junsong Yuan, Bo Li, and Kui Ren. Pointcloud saliency maps. In *Proceedings of the IEEE International Conference on Computer Vision*, pages 1598–1606, 2019.
- [49] Hang Zhou, Dongdong Chen, Jing Liao, Kejiang Chen, Xiaoyi Dong, Kunlin Liu, Weiming Zhang, Gang Hua, and Nenghai Yu. Lg-gan: Label guided adversarial network for flexible targeted attack of point cloud based deep networks. In *Proceedings of the IEEE/CVF Conference on Computer Vision and Pattern Recognition (CVPR)*, June 2020.
- [50] Hang Zhou, Dongdong Chen, Jing Liao, Kejiang Chen, Xiaoyi Dong, Kunlin Liu, Weiming Zhang, Gang Hua, and Nenghai Yu. Lg-gan: Label guided adversarial network for flexible targeted attack of point cloud based deep networks. In *Proceedings of the IEEE/CVF Conference on Computer Vision and Pattern Recognition*, pages 10356–10365, 2020.
- [51] Hang Zhou, Kejiang Chen, Weiming Zhang, Han Fang, Wenbo Zhou, and Nenghai Yu. Dup-net: Denoiser and upsampler network for 3d adversarial point clouds defense. In *Proceedings of the IEEE International Conference on Computer Vision*, pages 1961–1970, 2019.
- [52] Yi Zhu, Chenglin Miao, Foad Hajiaghajani, Mengdi Huai, Lu Su, and Chunming Qiao. Adversarial attacks against lidar semantic segmentation in autonomous driving. In *Proceedings of the 19th ACM Conference on Embedded Networked Sensor Systems*, pages 329–342, 2021.